J. Mol. Model. **1996**, *2*, 227 – 238

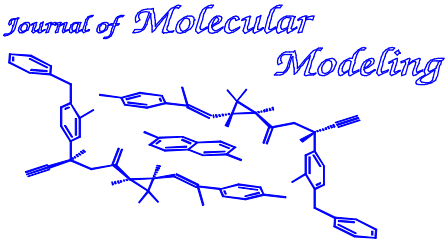

Sedimentation of Clusters of Spheres. I. Unconstrained Systems

Konrad Hinsen† and Gerald Reinhard Kneller*

Institut für Theoretische Physik A, RWTH Aachen, Templergraben 55, D-52056 Aachen, Germany (g.kneller@kfa-juelich.de)

† Present address: Institut de Biologie Structurale, Laboratoire de Dynamique Moleculaire, 41 Av. des Martyrs, F-38027 Grenoble, France (hinsen@ibs.ibs.fr)

Received: 14 May 1996 / Accepted: 1 August 1996 / Published: 4 September 1996

Abstract

We describe a numerical method for calculating hydrodynamic interactions between spherical particles efficiently and accurately, both for particles immersed in an infinite liquid and for systems with periodic boundary conditions. Our method is based on a multipole expansion in Cartesian tensors. We then show how to solve the equations of motion for translational and rotational motion of suspended particles at large Peclet numbers. As an example we study the sedimentation of an array of spheres with and without periodic boundary conditions. We also study the effect of perturbations on the stability of the trajectories.

Keywords: hydrodynamic interactions, Stokesian Dynamics simulations, colloids

Introduction

The behavior of particles suspended in a liquid has interested scientists ever since Stokes derived the drag formula for a single suspended sphere [1]. It is also important for many applications in rheology and colloid chemistry. Since all but the simplest problems require a numerical solution, numerical techniques play an important role in this field. In this article we deal with the two most important problems that any numerical simulation must address: the calculation of hydrodynamic interactions and the integration of the equations of motion.

In the treatment of hydrodynamic interactions, we limit ourselves to spherical particles and low Reynolds numbers, but aim to make the calculations both accurate and efficient. Hydrodynamic interactions have three properties that make their numerical treatment difficult:

- They are many-body interactions, i.e. they are not pairwise additive.
- They are long-ranged, decaying as $1/R$, where R is an interparticle distance. This creates special problems for periodic systems.
- They diverge for certain types of motion when particles approach each other.

The oldest and simplest approximation, apart from neglecting hydrodynamic interactions altogether, consists of assuming pairwise additivity and describing the interactions between each pair with the Oseen tensor (see Eq. 3.3). This describes the leading $1/R$ terms correctly, but is nevertheless very inaccurate. Besides, this approximation has the funda-

* *To whom correspondence should be addressed*

mental problem that the diffusion matrix is not positive definite, which can only be circumvented by introducing more arbitrary approximations [2]. Improvements such as the Rotne-Prager tensor are available, but they all share the basic problem of assuming pairwise additivity and not treating long-ranged contributions correctly; they also do not take rotational motion into account. The importance of the correct inclusion of all long-ranged terms was demonstrated in [3], where sedimentation of large rigid clusters of spheres was studied. Even in such rigid structures, where short-ranged lubrication forces are irrelevant, all terms decaying as $1/R^3$ or slower must be included to prevent dramatic errors in the sedimentation coefficient.

A better approximation has been developed by Durlofsky et al. [4]. Their scheme provides correct short-distance behavior and takes the multi-body nature of hydrodynamic interactions into account; however, it still does not contain all long-range terms correctly and does not provide sufficient accuracy for many applications. The first systematic scheme that can in principle be made arbitrarily accurate was proposed by Ladd [5, 6]. Both Durlofsky et al. [4] and Ladd [7] have used their methods for dynamical simulations.

Recently, Cichocki et al. [8] presented a number of improvements that yield accurate results at a much reduced cost. We will show how these improvements can be combined with previous analytical work on hydrodynamic interactions [9, 10] and numerical techniques from the related field of electrostatic interactions [11] to construct an efficient and accurate numerical implementation that calculates hydrodynamic interactions for systems of spherical particles. This implementation is available from the CPC library [12]. It has already been used in a study of the sedimentation coefficients of conglomerates of spheres [3], which has shown very good agreement with experimental results.

We will also present an integration scheme that is suitable for accurate dynamic simulations in the Stokesian Dynamics regime, i.e. at high Peclet numbers. We include the rotational motion of the particles, which has been neglected so far. The rotational motion of suspended spheres is often interesting in itself, but its calculation becomes essential when systems with constraints, such as rigid assemblies and flexible chains, are considered. We will deal with the specific problems of constrained systems in a second paper.

To test our integrator, we study the sedimentation of a few small systems, both in unbounded and periodic geometries. Unfortunately there is little experimental data we could compare to; the sedimentation of some small clusters has been studied by Jayaweera *et al.* [13], but they do not provide enough data to allow a meaningful comparison to numerical calculations. Therefore, we must limit ourselves to demonstrating the convergence of our results with decreasing time steps.

Stokesian Dynamics regime

We consider a system of N arbitrary particles suspended in a viscous liquid which is at rest at infinity. The particles move under the influence of external forces and forces mediated by the liquid; the latter consists of deterministic and random contributions. The equations of motion for the particles are given by

$$\frac{d}{dt}\left[\mathbf{MV}\right] = \mathbf{F}_h\left(\mathbf{R},\mathbf{V}\right) + \mathbf{F}_r\left(\mathbf{R}\right) + \mathbf{F}_{ext} \tag{2.1}$$

In this equation, $\mathbf{R}$ is a vector containing the positions and orientations of all particles. Similarly, $\mathbf{V}$ contains the translational and angular velocities, and $\mathbf{F}$ describes forces and torques. The matrix $\mathbf{M}$ is block diagonal and contains the masses and moments of inertia of all particles.

The vector $\mathbf{F}_h$ contains the hydrodynamic forces, i.e. the deterministic forces exerted by the fluid on the particle. We assume that they are given by

$$\mathbf{F}_h = -\boldsymbol{\zeta}\mathbf{V} \tag{2.2}$$

where the matrix $\boldsymbol{\zeta}$ is called *friction matrix* and depends on the viscosity of the liquid as well as on the positions and orientations of all suspended particles. The random forces $\mathbf{F}_r$ must be zero on average and fulfill the condition

$$\left\langle \mathbf{F}_r(0)\mathbf{F}_r(t)\right\rangle = kT\boldsymbol{\zeta}\delta(t) \tag{2.3}$$

which follows from the fluctuation-dissipation theorem.

Typically the time scale of observable particle motion is several orders of magnitude larger than the relaxation time of the particle momenta $\tau = m\zeta^{-1}$. In other words, the observed particle velocities, which we will denote by $\mathbf{U}$, are averages of the velocities $\mathbf{V}$ over times larger than τ. Under this condition, one can derive an expression for the displacement of the particles in a time interval Δt which is much larger than τ, but still small on the time scale a/U, where a is a typical particle size [14]. This expression is

$$\Delta\mathbf{R} = \boldsymbol{\mu}\mathbf{F}_{ext}\Delta t + \nabla\cdot\mathbf{D}\Delta t + \mathbf{X} \tag{2.4}$$

where $\boldsymbol{\mu} = \boldsymbol{\zeta}^{-1}$ is called the *mobility matrix* and $\mathbf{D} = kT\boldsymbol{\mu}$ is called the *diffusion matrix*. $\mathbf{X}$ is a random displacement with

$$\left\langle \mathbf{X}\right\rangle = 0 \quad , \quad \left\langle \mathbf{XX}\right\rangle = 2\mathbf{D}\Delta t \tag{2.5}$$

Simulations based on these equations are called *Brownian Dynamics* simulations.

To judge the relative importance of deterministic and the random motion, one introduces dimensionless quantities

$$\begin{aligned} \Delta\mathbf{R} &= a\Delta\hat{\mathbf{R}} \quad , \quad \mathbf{D} = D_0\hat{\mathbf{D}} \quad , \quad \mathbf{U} = U\hat{\mathbf{U}} \\ \Delta t &= \frac{a^2}{D_0}\Delta\hat{t} \quad , \quad \boldsymbol{\mu} = \frac{D_0}{kT}\hat{\boldsymbol{\mu}} \quad , \quad \mathbf{F}_{ext} = \frac{UkT}{D_0}\hat{\mathbf{F}}_{ext} \\ \nabla &= \frac{1}{a}\hat{\nabla} \quad , \quad \mathbf{X} = a\hat{\mathbf{X}} \end{aligned} \tag{2.6}$$

where a is the diameter of a typical particle, U a typical particle velocity, and D_0 a typical one-particle diffusion coefficient. Eq. 2.4 then becomes

$$\Delta\hat{\mathbf{R}} = \mathrm{Pe}\hat{\boldsymbol{\mu}}\hat{\mathbf{F}}_{ext}\Delta\hat{t} + \hat{\nabla}\cdot\hat{\mathbf{D}}\Delta\hat{t} + \hat{\mathbf{X}} \tag{2.7}$$

where the dimensionless quantity Pe = Ua/D_0 is called the *Peclet number.* At small Peclet numbers, Brownian motion dominates. At large Peclet numbers, the random displacements can be neglected. Simulations in this regime are called *Stokesian Dynamics* simulations.

From Eqs. 2.2, 2.3, and 2.4 it is evident that the effect of the liquid in which the particles are suspended is completely described by the friction matrix ζ or its inverse, the mobility matrix μ. An accurate and efficient calculation of these matrices is therefore extremely important for computer simulations of suspended particles.

Creeping flow and induced forces

Like most other approaches, our calculation of the friction and mobility matrices is based on the assumption that the liquid can be described by the so-called *creeping-flow equations*, which are valid for flow at low Reynolds numbers [15, 16]. We will also assume that the liquid is incompressible. The equations of motion for the liquid are then

$$\eta\nabla^2\mathbf{v} - \nabla p + \mathbf{f} = 0 \quad , \quad \nabla\cdot\mathbf{v} = 0 \tag{3.1}$$

where $\mathbf{v}(\mathbf{r})$ is the fluid velocity at point $\mathbf{r}$, $p(\mathbf{r})$ is the pressure, and $\mathbf{f}(\mathbf{r})$ is the force density acting on the fluid. In addition, boundary conditions at infinity and on the particle surfaces must be specified. Solutions to the creeping-flow equations for a given force density can be expressed conveniently as

$$\mathbf{v}(\mathbf{r}) = \mathbf{v}_0(\mathbf{r}) + \int d^3r'\,\mathbf{T}(\mathbf{r}-\mathbf{r}')\cdot\mathbf{f}(\mathbf{r}') \tag{3.2}$$

where $\mathbf{v}_0(\mathbf{r})$ is the solution for $\mathbf{f}(\mathbf{r})=0$ and the Green function $\mathbf{T}(\mathbf{r})$ for an unbounded fluid are given by the *Oseen tensor*

$$\mathbf{T}(\mathbf{r}) = \frac{1}{8\pi\eta}\left[\frac{1}{|\mathbf{r}|}\mathbf{1} + \frac{1}{|\mathbf{r}|^3}\mathbf{rr}\right] \tag{3.3}$$

Finally, we must specify the boundary conditions at the surfaces of the suspended particles and at infinity. Experience has shown that real systems are best described by *stick boundary conditions*, i.e. the fluid sticks to the particle surfaces. The flow at infinity depends on the problem being studied; the two most important cases are vanishing flow and uniform shear flow.

When the particles move relative to the fluid, they exert a force density on it, which for non-permeable particles is localized on the particle surfaces. The force density $\mathbf{f}(\mathbf{r};j)$ induced on particle j at position $\mathbf{R}_j$ moving with translational velocity $\mathbf{U}_j$ and angular velocity ω_j can be written as

$$\mathbf{f}(\mathbf{r};j) = \int d^3r'\,\mathbf{Z}_j(\mathbf{r}-\mathbf{R}_j,\mathbf{r}'-\mathbf{R}_j)\left[\mathbf{u}_j(\mathbf{r}') - \mathbf{v}_{aj}(\mathbf{r}')\right] \tag{3.4}$$

where $\mathbf{Z}_j(\mathbf{r},\mathbf{r}')$ is a friction kernel that depends only on properties of the particle and on the boundary conditions, $\mathbf{v}_{a,j}(\mathbf{r})$ is the velocity field in absence of particle j, and $\mathbf{u}_j(\mathbf{r})$ is given by

$$\mathbf{u}_j(\mathbf{r}) = \left[\mathbf{U}_j + \boldsymbol{\omega}_j\times(\mathbf{r}-\mathbf{R}_j)\right]\Theta(\mathbf{r}-\mathbf{R}_j) \tag{3.5}$$

where the step function $\Theta(\mathbf{r}-\mathbf{R}_j)$ is one inside the volume of the particle and zero outside. From Eq.3.2 it follows that the velocity field $\mathbf{v}_{a,j}$ is given by

$$\mathbf{v}_{a,j}(\mathbf{r}) = \mathbf{v}_0(\mathbf{r}) + \int d^3r'\,\mathbf{T}(\mathbf{r}-\mathbf{r}')\mathbf{f}(\mathbf{r}') \tag{3.6}$$

with

$$\mathbf{f}(\mathbf{r}) = \sum_i \mathbf{f}(\mathbf{r};i) \tag{3.7}$$

Calculation of the friction matrix

Eqs. 3.4 and 3.6 form an integral equation from which in principle $\mathbf{f}(\mathbf{r};i)$ can be determined for a given configuration of particles with given linear and angular velocities. Since the force and torque on particle i are related to $\mathbf{f}(\mathbf{r},i)$ by

$$\begin{aligned} \mathbf{F}_i &= \int d^3r\,\mathbf{f}(\mathbf{r};i) \\ \mathbf{T}_i &= \int d^3r(\mathbf{r}-\mathbf{R}_i)\times\mathbf{f}(\mathbf{r};i) \end{aligned} \tag{4.1}$$

and linear and angular velocities enter via Eq.3.5, the solution of the integral equation yields the friction matrix $\boldsymbol{\zeta}$.

To find a numerical solution of the integral equation, it must be transformed into an algebraic equation, which can be done with a multipole expansion analogous to the famil-

iar multipole expansion in electrostatic systems. As in electrostatics, the multipole expansion is guaranteed to converge only outside a spherical region containing all points where the force density does not vanish. It is therefore difficult to apply to non-spherical particles. For this reason, we will from now on restrict attention to particles of spherical shape. This is not as strong a restriction as it may seem, since many complicated shapes can be modelled by assemblies of small spherical components.

Multipole expansion

The multipole expansion for the induced force densities can be formulated in several ways; for numerical applications, the expansion in irreducible Cartesian tensors [17, 9, 10] is most convenient. The force multipole tensor of rank p+1 for particle j at position $\mathbf{R}_j$ is defined by

$$\mathbf{f}^{(p+1)}(j) = \frac{1}{p!}\int d^3r\left(\mathbf{r}-\mathbf{R}_j\right)^p \mathbf{f}\left(\mathbf{r}-\mathbf{R}_j;j\right) \tag{4.2}$$

Here $\mathbf{f}(\mathbf{r};j)$ is the force density induced on particle j, and $\mathbf{r}^p$ is the p-fold tensor product of the vector $\mathbf{r}$ with itself. Similarly, we define velocity multipole tensors that describe the velocity field $\mathbf{u}(\mathbf{r})$–$\mathbf{v}_0(\mathbf{r})$ around the particle by

$$\mathbf{c}^{(p+1)}(j) = \frac{1}{p!}\nabla^p\left[\mathbf{u}(\mathbf{r})-\mathbf{v}_0(\mathbf{r})\right]_{\mathbf{r}=\mathbf{R}_j} \tag{4.3}$$

These multipole tensors can be decomposed into irreducible tensors, of which many do not give a contribution to the flow field. It has been shown in [10] that it is sufficient to consider the irreducible tensors $\mathbf{f}_{l\sigma}$ and $\mathbf{c}_{l\sigma}$, l = 1,2,…, which for given l and σ have 2l + 1 independent components. These tensors are given by

$$\begin{aligned}
\left(\mathbf{f}_{l0}\right)_{\gamma_1\ldots\gamma_l} &= \overbrace{f^{(l)}_{\gamma_1\ldots\gamma_l}} \\
\left(\mathbf{f}_{l1}\right)_{\gamma_1\ldots\gamma_l} &= \frac{l}{l+1}\overbrace{\varepsilon_{\gamma_1\lambda\mu} f^{(l+1)}_{\lambda\gamma_2\ldots\gamma_l\mu}} \\
\left(\mathbf{f}_{l2}\right)_{\gamma_1\ldots\gamma_l} &= \frac{l(l+1)}{2(2l+1)}\overbrace{\delta_{\lambda\mu} f^{(l+2)}_{\lambda\mu\gamma_1\ldots\gamma_l}}
\end{aligned} \tag{4.4}$$

and

$$\begin{aligned}
\left(\mathbf{c}_{l0}\right)_{\gamma_1\ldots\gamma_l} &= \overbrace{c^{(l)}_{\gamma_1\ldots\gamma_l}} \\
\left(\mathbf{c}_{l1}\right)_{\gamma_1\ldots\gamma_l} &= l\overbrace{\varepsilon_{\gamma_1\lambda\mu} c^{(l+1)}_{\lambda\gamma_2\ldots\gamma_l\mu}} \\
\left(\mathbf{c}_{l2}\right)_{\gamma_1\ldots\gamma_l} &= l(l+1)\overbrace{\delta_{\lambda\mu} c^{(l+2)}_{\lambda\mu\gamma_1\ldots\gamma_l}}
\end{aligned} \tag{4.5}$$

where $\overbrace{\mathbf{a}}$ indicates the irreducible part of the tensor $\mathbf{a}$, $\varepsilon_{\alpha\lambda\mu}$ is the completely antisymmetric Levi-Cività tensor, and $\delta_{\alpha\beta}$ is the Kronecker symbol.

In this representation, the one-particle friction kernel $\mathbf{Z}_j(\mathbf{r},\mathbf{r}')$ is represented by a matrix $Z_{l\sigma\mu_1\ldots\mu_l,l'\sigma'\mu'_1\ldots\mu'_{l'}}(j)$ whose elements have been calculated for several particle models [18]. Similarly, the Oseen tensor is represented by a matrix $G_{l\sigma\mu_1\ldots\mu_l,l'\sigma'\mu'_1\ldots\mu'_{l'}}(ij)$, which expresses the flow field due to the force multipoles of particle j at the position of particle i. Expressions for its elements have been derived in [10]. The original integral equation for $\mathbf{f}(\mathbf{r};i)$ becomes a linear system of equations whose unknowns are the force multipole moments $\mathbf{f}_{l\sigma}$:

(4.6)

$$\mathbf{f}_{l\sigma}(i) = \sum_{\sigma'}\mathbf{Z}_{l\sigma\sigma'}(i)\left[\mathbf{c}_{l\sigma'}(i) - \frac{1}{l!}\sum_{j}\sum_{l''\sigma''}\mathbf{G}_{l\sigma';l''\sigma''}(ij)\cdot\mathbf{f}_{l''\sigma''}(j)\right]$$

The friction matrix can be obtained by solving these equations with $\mathbf{c}_{10}(j) = \mathbf{U}_j - \mathbf{v}_0(\mathbf{R}_j)$ and $\mathbf{c}_{11}(j) = 2\omega_j - \nabla\times\mathbf{v}_0(\mathbf{r})\big|_{\mathbf{r}=\mathbf{R}_j}$, making use of the fact that the forces $\mathbf{F}_j$ are given by $\mathbf{f}_{10}(j)$ and the torques $\mathbf{T}_j$ by $2\mathbf{f}_{11}(j)$. A detailed description of the multipole expansion can be found in [3] and [12]. It should be noted that the friction matrix resulting from this calculation is positive definite at all levels of truncation of the multipole expansion.

The core of our numerical scheme to calculate hydrodynamic interactions is the numerical solution of Eq. 4.6, truncated to a finite number of multipole moments. Details can be found in [12], where the implementation we use is described.

Short-distance forces

Relative motion of particles at short distances creates large frictional forces, whose description by a multipole expansion requires a prohibitively large number of terms. We therefore follow the suggestion of Durlofsky and Brady [4] and incorporate the short-range forces approximately in the form

$$\zeta^*_L = \zeta_L + \sum_{i,j=1}^{N}\left(\zeta^{(2)} - \zeta^{(2)}_L\right)_{ij} \tag{4.7}$$

where $\boldsymbol{\zeta}_L$ is the friction matrix as calculated according to the above description with a multipole expansion of order L, $\boldsymbol{\zeta}^{(2)}$ is the exact two-particle friction matrix calculated from lubrication theory [20], and $\boldsymbol{\zeta}_L{}^{(2)}$ is the two-particle friction matrix in order L approximation. The basic idea of this form is that the large short-range forces are localized in the region between two particles and can therefore be assumed to be pairwise additive. It is evident that $\boldsymbol{\zeta}^*{}_L$ converges to the same value for $L \to \infty$ as $\boldsymbol{\zeta}_L$, but it does so much faster. A multipole approximation of order 3 is sufficient to calculate the friction matrix with an accuracy of about 1% [8].

Mobility calculations

In most applications of hydrodynamic interaction, such as Stokesian Dynamics simulations, it is not the friction matrix that is immediately required, but the particle velocities resulting from a given set of external forces, i.e. $\boldsymbol{\mu}\cdot\mathbf{F}_{\text{ext}}$. These velocities can be obtained by first calculating the complete friction matrix and then solving the set of equations $\boldsymbol{\zeta}^*{}_L\mathbf{U} = \mathbf{F}_{\text{ext}}$ for $\mathbf{U}$. Indeed this has been done by Durlofsky et al. [4] and by Ladd [5]. However, it has been shown in [8] that the velocities can be obtained directly by solving a modification of the multipole equation that leads to the friction matrix. This procedure is numerically much more efficient.

Periodic boundary conditions

The long range of the hydrodynamic interactions causes both conceptual and practical problems when periodic systems are studied. The difficulties are exactly analogous to those for the equally long-ranged Coulomb interactions, and can be solved by very similar methods. Our treatment is based on the theoretical framework developed by Felderhof [21]. We limit ourselves to elementary cells of cubic shape.

In analogy to the fact that the electrostatic potential of a periodic system is defined only if the system as a whole is neutral, the velocity field in a periodic hydrodynamic system is finite only if the total force on it vanishes. If necessary this must be enforced by adding a neutralizing homogeneous force density to the system; this is physically equivalent to applying a constant pressure gradient. In addition, the shape of the macroscopic assembly of elementary cells whose infinite limit is to be considered must be specified; we will assume it to be spherical.

Such a system can be treated much like a finite one with a different Green function [21]. The Oseen tensor $\mathbf{T}(\mathbf{r})$ must be replaced by the tensor

$$\mathbf{T}_H(\mathbf{r}) = \tfrac{1}{4\pi\eta}\left[S_1(\mathbf{r}) - \nabla\nabla S_2(\mathbf{r})\right] \tag{5.1}$$

which was first introduced by Hasimoto [22]. The functions S_1 and S_2 have cubic symmetry and satisfy the equations

$$\begin{aligned}\nabla^2 S_1 &= -4\pi\left[\sum_n \delta(\mathbf{r}-\mathbf{n}L) - \frac{1}{V}\right]\\ \nabla^2 S_2 &= S_1\end{aligned} \tag{5.2}$$

where L is the edge length of the elementary cell and V its volume. A method for the efficient calculation of S_1 and S_2, based on an analogous method for electrostatics [23], is given in [24]. It should be noted that the Hasimoto tensor (5.1) already includes the effect of the neutralizing homogeneous force density added to make the velocity field finite.

The multipole expansion in terms of irreducible Cartesian tensors that has been mentioned before must be re-derived with the new Green function. In its original form, it is valid only when the applied force density vanishes outside the particles. This assumption is violated by the addition of the neutralizing homogeneous force density. Starting from the original Taylor expansion that leads to Eq. 4.2, one finds again the formula given in [12] with the matrix $G(ij)$ replaced by

$$G_P(ij) = G_H(ij) + G'(ij) - G''(ij) \tag{5.3}$$

Here $G_H(ij)$ is the result of evaluating Eq.(A6) from [3] or Eq. (A.13) from [12] with the Oseen tensor $\mathbf{T}(\mathbf{r})$ replaced by the Hasimoto tensor $\mathbf{T}_H(\mathbf{r})$. The only non-zero elements of $G'(ij)$ are

$$\begin{aligned}G'_{10\mu;12\mu'}(ij) &= \tfrac{2}{3\eta}\\ G'_{11\mu;11\mu'}(ij) &= -\tfrac{2}{3\eta}\\ G'_{12\mu;10\mu'}(ij) &= G'_{00\mu;02\mu'}(ij)\\ G'_{20\mu_1\mu_2;20\mu'_1\mu'_2}(ij) &= -\tfrac{1}{5\eta}\end{aligned} \tag{5.4}$$

Note that $G'(ij)$ is non-zero even for $i = j$. The matrix $G''(ij)$ is zero for $i = j$ and for $i \neq j$ given by Eq. (A6) from [3] with $\mathbf{T}(\mathbf{r})$ replaced by

$$\mathbf{T}''(\mathbf{r}) = \tfrac{1}{6\eta}\mathbf{r}^2\mathbf{1} - \tfrac{1}{120\eta}\nabla\nabla\left(\mathbf{r}^2\right)^2 \tag{5.5}$$

and evaluated at $\mathbf{r} = 0$.

For $l + l' > 4$ the elements of $G_P(ij)$ are lattice sums over the corresponding elements of $G(ij)$; in numerical calculations, they can be obtained by summing over all lattice sites within a cutoff radius. The remaining elements contain long-ranged contributions and must be calculated by evaluating the functions $S_1(\mathbf{r})$ and $S_2(\mathbf{r})$ as described in [24] and using the procedure described above.

Stokesian Dynamics

Equations of motion

In the Stokesian Dynamics regime, i.e. for high Peclet numbers (see Eq. 2.7), only the external forces need to be considered as driving forces for the particle displacements, and Eq. 2.4 becomes

$$\Delta\mathbf{R} = \boldsymbol{\mu}\mathbf{F}_{ext}\Delta t \tag{6.1}$$

In principle this formula can be used to calculate particle trajectories. It is the Euler integration scheme [25] for the differential equation

$$\dot{\mathbf{R}} = \boldsymbol{\mu}\mathbf{F}_{ext} \tag{6.2}$$

However, the Euler scheme is not ideal for numerical purposes. Other methods are more stable and more accurate at the same computational cost [25].

If rotational degrees of freedom are to be integrated, Eq. 6.2 must be generalized. The velocity vector replacing $\dot{\mathbf{R}}$ then contains all translational velocities, $\mathbf{V}_1,...,\mathbf{V}_N$, and all angular velocities, $\boldsymbol{\omega}_1,\ldots,\boldsymbol{\omega}_N$, of the particles. Correspondingly, $\mathbf{R}$ contains the particle positions, specified by $\mathbf{R}_1,\ldots,\mathbf{R}_N$, and the orientations, specified by $\mathbf{Q}_1,\ldots,\mathbf{Q}_N$, where $\mathbf{Q}$ is a suitable set of angular variables. $\mathbf{F}_{ext}$ is the vector of all external forces, $\mathbf{F}_1,\ldots,\mathbf{F}_N$, and all external torques, $\mathbf{T}_1,\ldots,\mathbf{T}_N$. Using the above definitions, the equations of motion for Stokesian Dynamics read explicitly

$$\mathbf{V}_i = \sum_{j=1}^{N} \boldsymbol{\mu}_{ij}^{tt}\mathbf{F}_j + \sum_{j=1}^{N} \boldsymbol{\mu}_{ij}^{tr}\mathbf{T}_j \tag{6.3}$$

$$\boldsymbol{\omega}_i = \sum_{j=1}^{N} \boldsymbol{\mu}_{ij}^{rt}\mathbf{F}_j + \sum_{j=1}^{N} \boldsymbol{\mu}_{ij}^{rr}\mathbf{T}_j \tag{6.4}$$

$$\dot{\mathbf{R}}_i = \mathbf{V}_i \tag{6.5}$$

$$\dot{\mathbf{Q}}_i = \mathbf{B}(\mathbf{Q}_i)\,\boldsymbol{\omega}_i \tag{6.6}$$

where $\boldsymbol{\mu}_{ij}^{tt}$, $\boldsymbol{\mu}_{ij}^{tr} = \boldsymbol{\mu}_{ji}^{rt}$, and $\boldsymbol{\mu}_{ij}^{rr}$ are 3 × 3 submatrices of the mobility matrix $\boldsymbol{\mu}$. The linear relation (6.6) between the angular velocities and the time derivatives of the angular coordinates depends on the choice of the latter. The equations of motion (6.3) — (6.6) may be written in the compact form

$$\dot{\mathbf{R}} = \mathbf{B}\boldsymbol{\mu}\mathbf{F}_{ext} \tag{6.7}$$

where $\mathbf{B}$ is a block-diagonal matrix containing unit matrices for the mapping $\mathbf{V}_i \rightarrow \dot{\mathbf{R}}_i$ and the matrices $\mathbf{B}(\mathbf{Q}_i)$ for the mapping $\boldsymbol{\omega}_i \rightarrow \dot{\mathbf{Q}}_i$.

It is well known from molecular dynamics simulations that quaternion parameters are a convenient choice for the angular variables, since the resulting matrices $\mathbf{B}(\mathbf{Q}_i)$ are singularity-free [26]. A comprehensive treatise on quaternions and their relations to spatial rotations can be found in [27]. Here it is sufficient to know that rotations can be parameterized in terms of four real numbers, q_0, q_1, q_2, q_3, which are subject to the normalization condition $q_o^2 + q_1^2 + q_2^2 + q_3^2 = 1$. For quaternion parameters the relation (6.6) reads explicitly (the particle index has been dropped) [28]:

$$\begin{pmatrix} \dot{q}_0 \\ \dot{q}_1 \\ \dot{q}_2 \\ \dot{q}_3 \end{pmatrix} = \frac{1}{2}\cdot \begin{pmatrix} -q_1 & -q_2 & -q_3 \\ q_0 & q_3 & -q_2 \\ -q_3 & q_0 & q_1 \\ q_2 & -q_1 & q_0 \end{pmatrix} \begin{pmatrix} \omega_x \\ \omega_y \\ \omega_z \end{pmatrix} \tag{6.8}$$

Here the angular velocity components refer to the *laboratory-fixed* coordinate system. Eq. 6.8 is consistent with the normalization of the quaternion components, since

$$q_o\dot{q}_o + q_1\dot{q}_1 + q_2\dot{q}_2 + q_3\dot{q}_3 = \tfrac{1}{2}\cdot\frac{d}{dt}\left(q_0^2 + q_1^2 + q_2^2 + q_3^2\right) = 0$$

for any set of angular velocity components.

Integration of the equations of motion

Translational motion. Due to the singular behavior of the hydrodynamic interactions at short distances [20, 16] the dynamics of suspended particles can exhibit very different time scales, since relative motion for particles which are in close contact is almost completely suppressed. Differential equations describing such dynamical systems are called *stiff differential equations*. In practice so-called implicit algorithms have proven to be most useful to integrate stiff differential equations [25,29]; we find this confirmed for our case, for which we compared explicit and implicit central difference schemes for both translational and rotational motion. In the case of translation, the trajectories of particles in close contact showed unstable oscillatory relative motions, ending with unphysical overlaps, when an explicit scheme was used. This could be avoided by using the following discretized form for the translational equation of motion:

$$\dot{\mathbf{R}}_i(n) \approx \frac{\mathbf{R}_i(n+1) - \mathbf{R}_i(n-1)}{2\Delta t} = \mathbf{V}_i\left(\left\{\overline{\mathbf{R}}_j\right\}\right) \tag{6.9}$$

where $\mathbf{V}_i$ given by Eq. 6.3 and the positions $\bar{\mathbf{R}}_j$ by

$$\bar{\mathbf{R}}_j = \tfrac{1}{2}\Big(\mathbf{R}_j(n) + \tfrac{1}{2}\big[\mathbf{R}_j(n+1) + \mathbf{R}_j(n-1)\big]\Big) \tag{6.10}$$

The arguments n, n+1, and n–1 are shorthands for $t = n \cdot \Delta t$ etc. Note that the $\bar{\mathbf{R}}_j$ depend on the new positions $\mathbf{R}_j(n+1)$. This leads to the following iterative update for the particle positions:

$$\mathbf{R}_i^{\nu+1}(n+1) = \mathbf{R}_i(n-1) + 2\Delta t \mathbf{V}_i\left(\left\{\bar{\mathbf{R}}_j^{\nu}\right\}\right) \tag{6.11}$$

The superscript ν in $\bar{\mathbf{R}}_j^{\nu}$ indicates that the iterated positions $\mathbf{R}_i^{\nu}(n+1)$ are to be used in the evaluation of the positions $\bar{\mathbf{R}}_j$. We start the iteration procedure with

$$\mathbf{R}_j^0(n+1) = 2\mathbf{R}_j(n) - \mathbf{R}_j(n-1) \tag{6.12}$$

This corresponds to setting $\bar{\mathbf{R}}_j = \mathbf{R}_j(n)$, which is the conventional central difference scheme. The iteration was stopped when the Euclidian norm of the distance between consecutive estimates for $\mathbf{R}_j(n+1)$ was below a prescribed tolerance limit $\varepsilon \cdot a$, with a being the particle radius. It should be noted that the implicit scheme described here is not essential as long as all the particle distances are sufficiently large; we found that for distances larger than $10^{-8}a$ the standard explicit scheme can be used without any problems.

Rotational motion. We found that the rotational motion, for which the singularities in the hydrodynamic interactions at short distances are weaker, could be sufficiently well integrated with a normal central difference scheme. In analogy to Eq. 6.9, the discretized form of the rotational equation of motion reads

$$\dot{\mathbf{Q}}_i(n) \approx \frac{\mathbf{Q}_i(n+1) - \mathbf{Q}_i(n-1)}{2\Delta t} = \mathbf{B}\big(\mathbf{Q}_i(n)\big)\boldsymbol{\omega}_i\Big(\big\{\mathbf{R}_j(n)\big\}\Big) \tag{6.13}$$

yielding the update formula

$$\mathbf{Q}_i(n+1) = \mathbf{Q}_i(n-1) + 2\Delta t \mathbf{B}\big(\mathbf{Q}_i(n)\big)\boldsymbol{\omega}_i\Big(\big\{\mathbf{R}_j(n)\big\}\Big) \tag{6.14}$$

for the quaternion parameters. The angular velocities $\boldsymbol{\omega}_i$ are determined by Eq. 6.4. The body-fixed basis vectors $\mathbf{e'}_i$ rotating with the spheres can be updated using $\mathbf{e'}_i(n+1) = \mathbf{U}(\mathbf{Q}_i[n+1]) \cdot \mathbf{e'}_i(0)$, where $\mathbf{U}(\mathbf{Q})$ is the rotation matrix

$$\mathbf{U}(\mathbf{Q}) = \begin{pmatrix} q_0^2 + q_1^2 - q_2^2 - q_3^2 & 2(-q_0q_3 + q_1q_2) & 2(q_oq_2 + q_1q_3) \\ 2(q_0q_3 + q_1q_2) & q_0^2 + q_2^2 - q_1^2 - q_3^2 & 2(-q_0q_1 + q_2q_3) \\ 2(-q_0q_2 + q_1q_3) & 2(q_0q_1 + q_2q_3) & q_0^2 + q_3^2 - q_1^2 - q_2^2 \end{pmatrix}$$

Close contacts A problem one has to face with iterative integration schemes for differential equations is slow convergence. In our case this concerns the update of the particle positions (see Eq. 6.11). Slow convergence can occur in situations where the system asymptotically approaches a configuration in wich particles stick to each other (see our example below). We found that sometimes 50 iterations and more were necessary for $\varepsilon \approx 10^{-12}$, whereas for larger, but still small, particle separations only two or three iterations were necessary. Due to inaccuracies inherent in any numerical integration scheme even the unphysical situation of overlapping spheres cannot not be excluded. To solve the problem of slow convergence and unphysical particle overlaps, we removed critical close contacts by the following algorithm:

1. Find all pairs (i,j) of particles whose distance is less or equal to $2a\cdot(1+\varepsilon)$, where a is the particle radius and ε is a tolerance limit.
2. Find all clusters of particles which have a connection *via* close contacts. Consider e.g. three particles 1,2,4 where (1,2) and (2,4) are in close contact. Then, according to the above definition, {1,2,4} form a cluster since there is a path from 1 to 4: 1 – 2 – 4.
3. Find the centroid $\mathbf{R} = 1/N\ \Sigma_{(i)}\mathbf{R}_i$ for each cluster and scale the relative positions by $1 + 2\varepsilon$. Here N is the number of particles in a cluster. The new positions are then given by $\mathbf{R'}_i = \mathbf{R} + (1 + 2\varepsilon)(\mathbf{R}_i - \mathbf{R})$.
4. Goto 1, to check if new contacts with particles not yet involved in close contacts have been created by steps 1 to 3. If this is the case, *add* these contacts to the ones found in 1 and proceed with 2.

The procedure described above terminates after a finite number of cycles. The extreme case which can occur is that the whole system is treated as one cluster. We emphasize that the above procedure should only be used if the numerical solution fails due to inevitable accuracy problems. It is no substitute for an implicit integration scheme which can handle much closer contacts than an explicit scheme.

Accuracy. We determined the accuracy of the explicit and implicit integration schemes by simulating the sedimentation of three particles in a linear arrangement with different time steps. Here and in the following section, we use a dimensionless unit of time defined such that a single sphere in an unbounded liquid would move a distance of $2a/3$ in a time interval of length 1. Figure 1 show the differences in vertical position for the central particle. All differences are

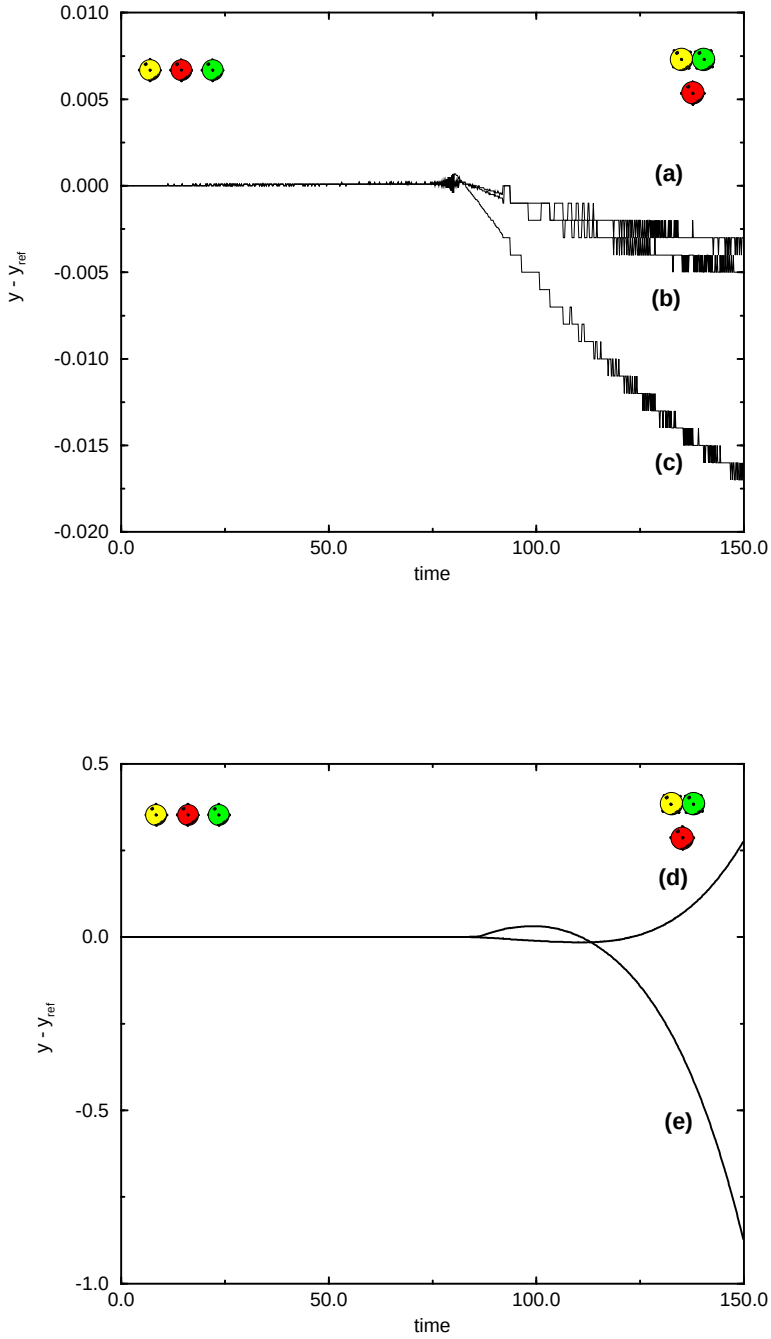

Figure 1. *The dependence of the error on the integration step. (a) Explicit/implicit integrator, Δt = 0.001. (b) Explicit/implicit integrator, Δt = 0.01. (c) Explicit/implicit integrator, Δt = 0.05. (d) Explicit integrator, Δt = 0.001. (e) Explicit integrator, Δt = 0.005.*

with respect to a reference run with a time step of $\Delta t = 0.001$ using the the implicit integrator at all times. The initial and final configurations are shown in the figures.

Figure 1, curves a – c show the results for an integration that uses the implicit integrator whenever a distance becomes smaller than 0.001 *a*. Initially, while all particle distances are large, the errors are negligible. The correction mechanism described above becomes active around $t = 80$, when the two outer spheres approach each other significantly. Nevertheless the absolute error remains small even for the largest time step, $\Delta t = 0.05$. The step structure of the error is caused by the close contact elimination procedure described in the last section.

The corresponding curves (d – e) for a purely explicit integration scheme (Figure 1b) show that the error in this case already becomes very large for small step sizes (note the different scale). This demonstrates the necessity of the implicit integration scheme whenever short distances cannot be excluded.

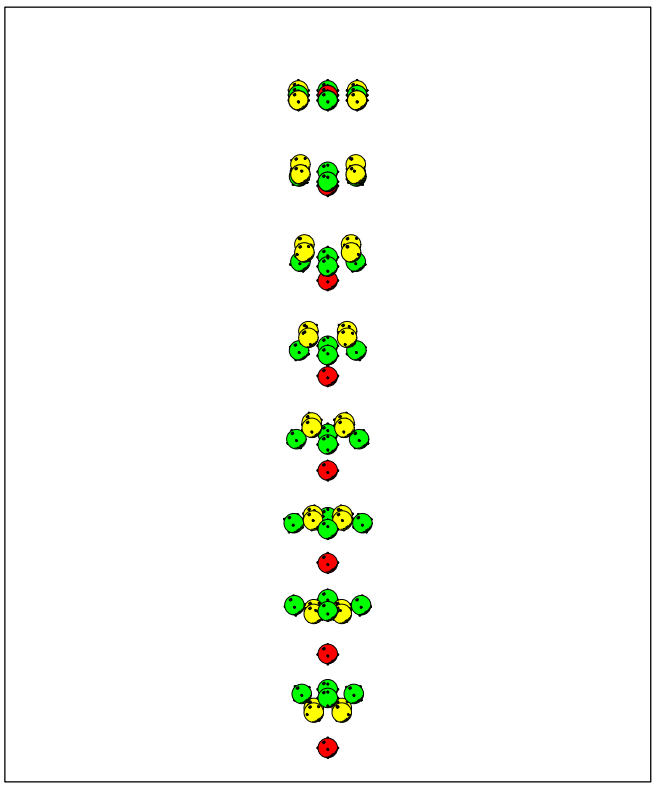

Figure 2. *Sedimentation of a planar square array of nine equal spheres in a viscous liquid under the influence of a constant gravitational force. The time separation between two consecutive configurations is* $\Delta t_{frame} = 5$*, corresponding to 5000 time steps of length* $\Delta t = 0.001$*. A single particle would move* $2/3 \cdot 10^{-3}a$ *during a time step, where a is the sphere's radius.*

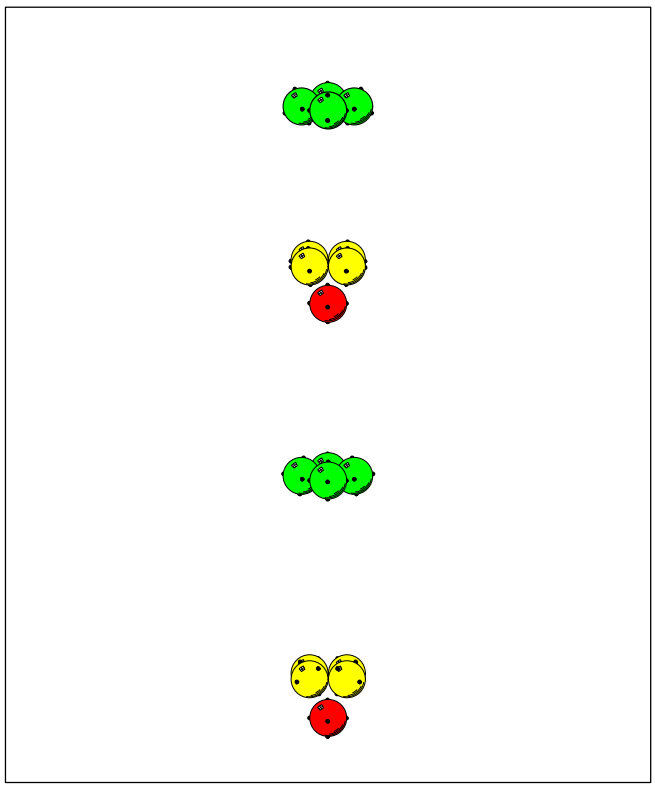

Figure 3. *The end of the simulation whose beginning is shown in Figure 1. The two configurations correspond to* $t = 135$ *and* $t = 150$*, respectively.*

Examples

As an example we study the sedimentation of a square array of nine equal spheres in a viscous liquid under the influence of gravity — see video sequence no. Ia ('Nine equally sized spheres starting on a quadratic grid'). Here and in all following video sequences *the center of mass motion is subtracted*. The overall sedimentation of the cluster is shown on the lefthand side of the screen. The height of the frame indicates the total falling distance, and the height of the black bar corresponds approximately to the height of the screen.

Figure 2 shows the beginning of the simulation. The start configuration is shown at the top: the nine spheres are located in a plane perpendicular to the direction of gravity; the center-to-center distance between nearest neighbours is 3a, where a is the radius of a sphere. There are no interactions between the particles in addition to the hydrodynamic forces.

We ran a simulation of this system for 150,000 time steps using the methods described above. The length of each time step was $\Delta t = 0.001$ in our units. Figure 2 shows eight configurations at time intervals of 5, beginning with the initial configuration. Figure 3 shows two configurations from the end of the simulation run, corresponding to times $t = 135$ and $t = 150$, respectively. In both pictures, we use three different colours to mark groups of spheres related by symmetry with respect to a 90° rotation around the central sphere in the initial configuration. The small dots are added to show the rotation of the spheres. The positions of the configurations in the pictures correspond to the actual distance they have moved.

In the beginning of the simulation the particles separate into three planes, the corner particles being the slowest and the center one being the fastest. This reflects the different exposure of the particles to the surrounding liquid. Then the edge particles move outward and the corner particles inward, whereupon they "dive" through the plane formed by the former edge particles. Meanwhile the center particle seems to escape from the others. In the part between Figure 2 and Figure 3 (see video sequence no. Ia), the edge particles in turn dive through the plane of the corner particles. This interchange of the planes is not periodic, however; finally the corner and center particles form a quasi-rigid cluster of five

Figure 4. *The time evolution of the rotation angles.*

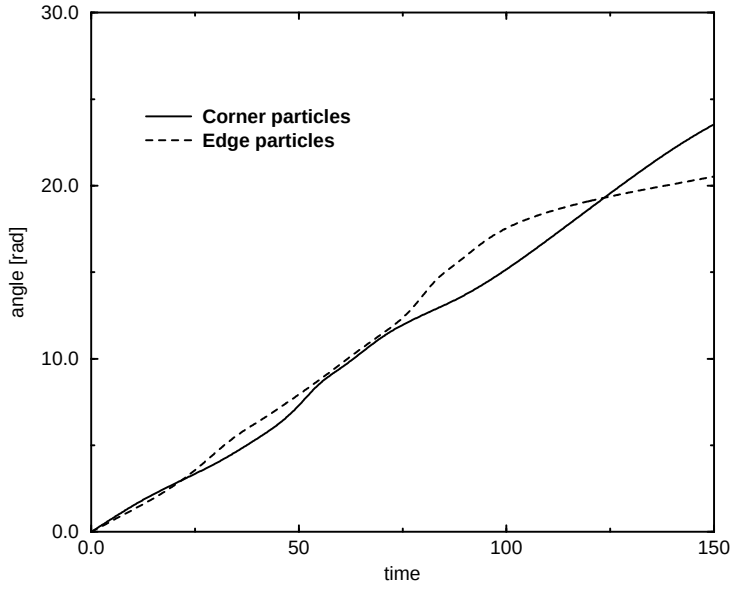

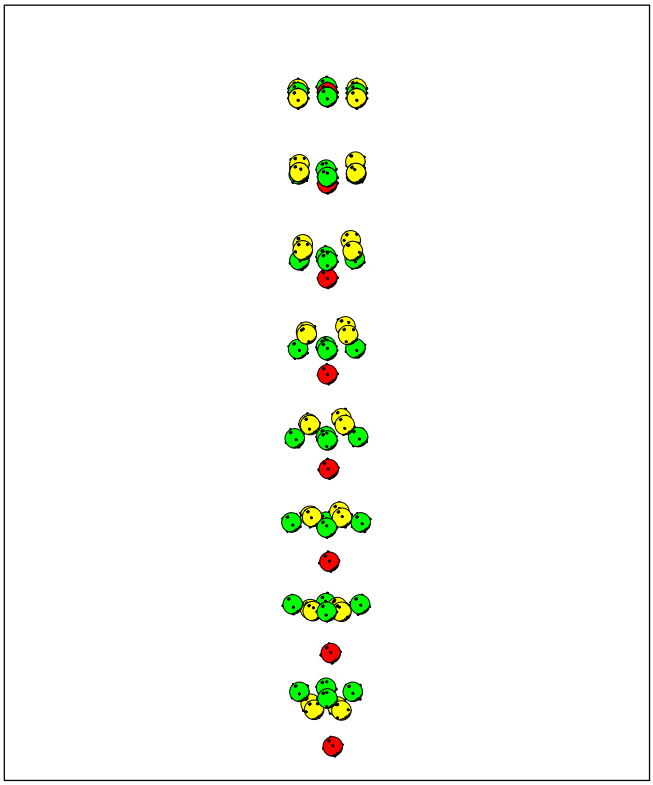

Figure 5. *The beginning of a simulation with a slightly perturbed initial configuration. The time separation between two consecutive configurations is the same as in Figure 1, i.e.* $\Delta t_{frame} = 5$. *The simulation time step is ten times as large as in the simulation shown in Figures 1 and 2, i.e.* $\Delta t = 0.01$.

particles falling somewhat faster than the second cluster consisting of the four former edge particles in close contact.

The angle of rotation of the corner and edge particles in the course of the simulation is shown in Figure 4. Note that the axis of rotation is constant for each particle, so that a single angle is sufficient to characterize the rotational motion.

To test the stability of the system with respect to small perturbations of the initial configuration, we ran a second simulation in which all the initial particle coordinates were randomly shifted by ± 0.1 *a*. This simulation was run with a time step of $\Delta t = 0.01$. The results are shown in video sequence no. Ib ('9 equally sized spheres starting on a slightly perturbed quadratic grid') and in Figures 5 (first part) and 6 (second part). For comparison, the total falling height indicated by the frame is the same as in the simulation shown in video sequence no. Ia. Until approximately $t = 80$ the configurations resemble those of the unperturbed simulation, but then the order is quickly destroyed.

The strong influence of the long-range terms in the hydrodynamic interactions can be seen by comparing a simulation of a system with and without periodic boundary conditions — see video sequence no. Ic ('Nine equally sized spheres starting on a quadratic grid with periodic boundary conditions'). For comparison, the total falling height indicated by the frame is again the same as in the simulation shown in video sequence no. Ia.

The nine particles now form the cubic elementary cell of a periodic system whose lattice constant L is $16a$ ($L = 16$ in our units). This simulation was also run with a time step of $\Delta t = 0.01$. The beginning of the simulation is shown in Figure 7. It should be noted that the time separation between

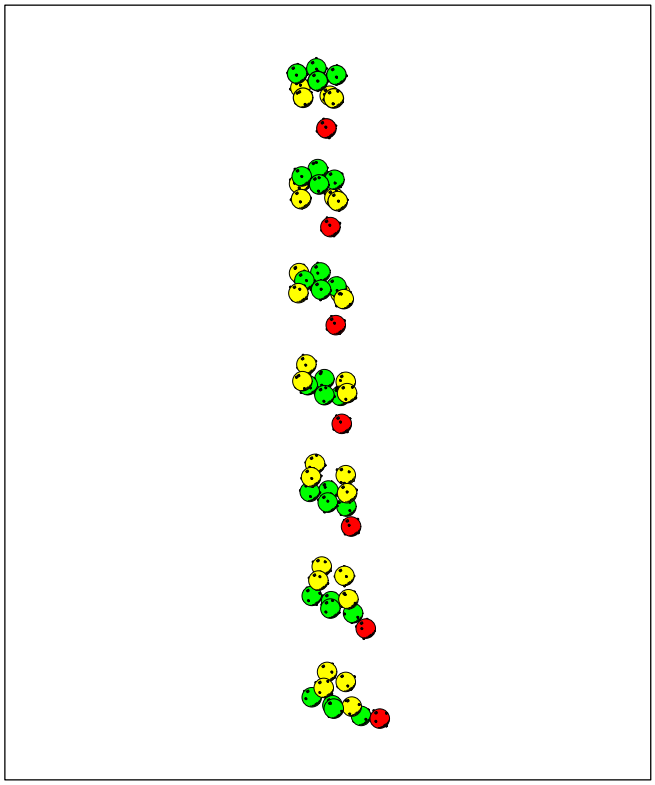

Figure 6. *The continuation of Figure 4.*

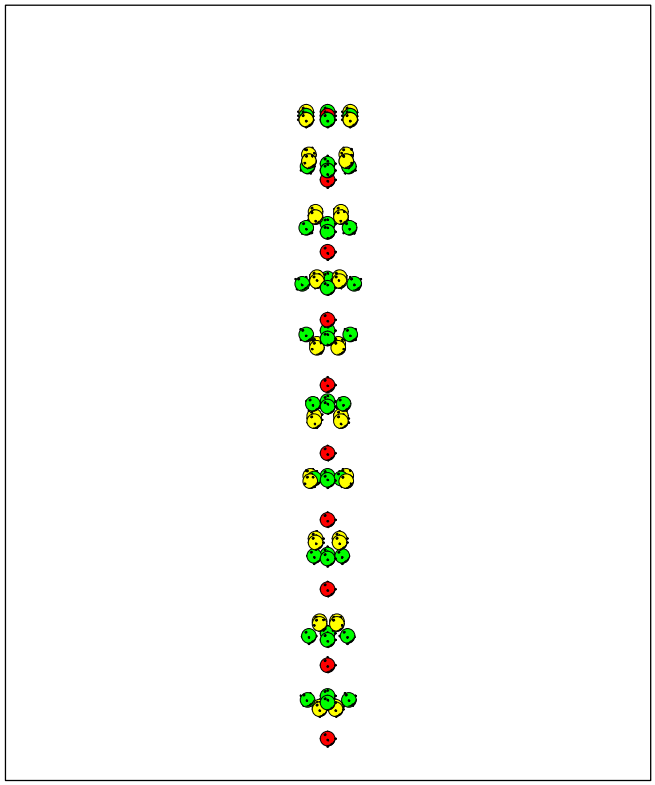

Figure 7. *The beginning of a simulation with periodic boundary conditions. Only one elementary cell is shown. The edge of the elementary cell has a length L of 16a (L = 16 in our units), where a is the radius of the spheres. Note that the time separation of two subsequent configurations is twice as much as in Figure 2, i.e.* $\Delta t_{frame} = 10$. *The simulation time step is* $\Delta t = 0.01$.

two consecutive configurations in this picture is twice as large as in Figure 2; the net sedimentation of the particles is much slower than in the non-periodic case. Nevertheless, the relative motion of the spheres with respect to one another is not much influenced by the presence of the periodic images.

Figure 8 shows the heat produced as the particles move downward against the friction caused by the liquid for all three simulations. The heat production is given by

$$\sum_i \mathbf{F}_i \cdot \mathrm{v}_i \qquad (7.1)$$

the rotational velocities do not enter as there are no applied torques. For the periodic system, only one of the images is used. We normalize the heat production by that of nine spheres sedimenting at infinite distance. Since in our simulation the forces on all particles are identical and constant, the heat production is proportional to the velocity of the center of mass of the nine spheres. Figure 8 shows that initially the heat production increases but is modulated by an oscillation corresponding to the position interchanges of the planes of the corner and edge particles. But once the final clusters are formed, the heat production decreases monotonously. This figure also illustrates the differences between the three simulations quantitatively. It can clearly be seen where the perturbed simulation starts to deviate significantly from the unperturbed one, and the smaller sedimentation speed of the periodic system is also evident.

This example shows that even very simple systems with hydrodynamic interactions can show a surprisingly complicated behavior. We are not aware of any theory that could predict more than the very first steps of our simulations.

Conclusion

We have shown how the hydrodynamic forces between spherical particles immersed in a liquid can be treated numerically, and how Stokesian Dynamics simulations can be performed on such systems. To demonstrate our method, we have performed a simulation of a simple model system.

In its current state, our method can be used to study the dynamics of colloidal suspensions, provided that the Peclet number is high enough to justify Stokesian Dynamics. It can

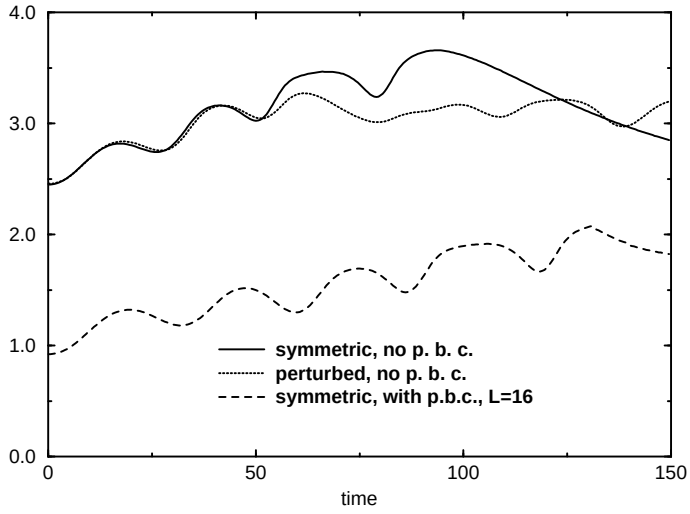

Figure 8. *The normalized heat production in the course of the three simulation runs.*

also be used for Monte-Carlo type calculations of equilibrium properties irrespective of the Peclet number. One of the most interesting applications from our point of view is the simulation of macromolecules modelled as assemblies of spheres; however, this necessitates the treatment of geometrical constraints, which we will present in a separate article.

So far we have not mentioned systems at low Peclet numbers. For such systems, all terms in Eq. 2.4 must be taken into account. This has been done in [14], but only for translational motion and the Oseen-tensor approximation for the mobility matrix. The generalization to an accurate description of finite particles remains an interesting challenge.

Acknowledgement We wish to thank the Zentralinsitut für Angewandte Mathematik of the KFA Jülich, in particular Klaudia Waschbüsch and Maik Boltes, for producing the video sequences shown in this article. The single frames were generated with the program MOLSCRIPT [30]. One of us (GRK) wishes to thank the German Space Agency for financial support.

References

1. Stokes, G.G. *Trans. Cambridge Philos. Soc.* **1851**, *9*, 8.
2. Dickinson, E. *Chem. Soc. Rev*. **1985**, *14*, 421.
3. Cichocki, B.; Hinsen, K. *Phys. Fluids* **1985**, *7*, 286.
4. Durlofsky, L; Brady, J; Bossis, G. *J. Fluid Mech.* **1987**, *180*, 21.
5. Ladd, A.J.C. *J. Chem. Phys.* **1988**, *88*, 5051.
6. Ladd, A.J.C. *J. Chem. Phys.* **1989**, *90*, 1149.
7. Ladd, A.J.C. *Phys. Fluids* **1993**, *A5*, 299.
8. Cichocki, B; Felderhof, B.U.; Hinsen, K; Wajnryb, E; Blawzdziewicz, J. *J. Chem. Phys.* **1994**, *100*, 3780.
9. Schmitz, R. *Die effektive Viskosität flüssiger Suspensionen*, PhD thesis, RWTH Aachen, **1980**.
10. Schmitz, R. *Physica*, **1980**, *A102*, 161.
11. Hinsen, K.; Felderhof, B.U. *J. Math. Phys.* **1992**, *33*, 3731.
12. Hinsen, K. *Comp. Phys. Comm.* **1995**, *88*, 327.
13. Jayaweera, K.O.L.F.; Mason, B.J.; Slack, G.W. *J. Fluid Mech.* **1964**, *20*, 121.
14. Ermak, D.L.; McCammon, J.A. *J. Chem. Phys.* **1978**, *69*, 1352.
15. Happel, J.; Brenner, H. *Low Reynolds number hydrodynamics*, Noordhoff, Leyden, **1973**.
16. Kim, S.; Karrila, S.J. *Microhydrodynamics*, Butterworth-Heinemann, Boston, **1991**.
17. Schmitz, R.; Felderhof, B.U. *Physica* **1978**, *A92*, 423.
18. Cichocki, B.; Felderhof, B.U.; Schmitz, R. *Physico-Chemical Hydrodynamics* **1988**, *10*, 383.
19. Cipriani, J; Silvi, B. *Mol. Phys.* **1982**, *45*, 259.
20. Jeffrey, D.J.; Onishi, Y. *J. Fluid Mech.* **1984**, *139*, 261.
21. Felderhof, B.U. *Physica* **1989**, *A159*, 1.
22. Hasimoto, H. *J. Fluid Mech.* **1959**, *5*, 317.
23. Cichocki, B.; Felderhof, B.U.; Hinsen, K. *Phys. Rev. 1989*, **A39**, 5350.
24. Cichocki ,B.; Felderhof, B.U. *Physica* **1989**, *A159*, 19.
25. Press, W.H.; Teukolsky, S.A.; Vetterling, W.T.; Flannery, B.P. *Numerical Recipes in C* (second edition), Cambridge University Press, Cambridge, **1992**.
26. Evans, D.J.; Murad, S. *Mol. Phys.* **1977**, *34*, 327.
27. *Altmann*, B. *Rotations, Quaternions, and Double Groups*, Clarendon Press, Oxford, **1986**.
28. Kneller, G.; Geiger, A. *Molecular Simulation* **1989**, *3*, 283.
29. Stoer, J.; Bulirsch, R. *Introduction to numerical analysis*, Springer, Berlin, New York, **1980**.
30. Kraulis, P.J. *J. Appl. Cryst.* **1991**, *24*, 946.